Aspect Ratio Requirements for Nanotube-Reinforced, Polymer-Matrix Composites[☆]

J.A.Nairn

Wood Science and Engineering, Oregon State University, Corvallis, OR 97330, USA

Abstract

A fiber's efficiency in a short-fiber composite can be accurately solved by shear-lag methods, which can account for fiber geometry, an imperfect interface (or interphase), and extend to low volume fractions. Such an analysis was used to evaluate the aspect ratio requirements for single-walled nanotubes (SWNT) in a polymeric composite and contrast it to conventional fibers. The aspect ratio requirements are indistinguishable among all stiff fibers, except at low volume fractions where stiffer fibers require higher aspect ratios. The required aspect ratio decreases significantly at higher volume fractions. A scaling effect in the interphase term implies the interphase is more important for nano-fibers than for larger fibers. If the interface between nano-fibers and the matrix is not excellent, those fibers will not provide effective reinforcement. The most promising SWNT composites should use higher volume fractions and focus on systems where the fiber can stiffen the matrix in the interphase region.

Key words: A. Fibres, B. Nano-structures, C. Interface/interphase, D. Analytical modelling

1. Introduction

A common model for aligned short-fiber composite modulus, E_c^*, simply modifies the standard rule of mixtures [1, 2]. For nanotubes reinforcement, this model takes the form

$$E_c^* = \eta_f E_{zz}^{(f)} \phi V_f + E_m V_m \tag{1}$$

where η_f is a fiber efficiency factor, $E_{zz}^{(f)}$ is the nanotube wall axial modulus, E_m is the matrix modulus, and V_f and V_m are the fiber and matrix volume fractions. The fiber volume fraction is taken as *inclusive* of the hollow space within the nanotubes (for better comparison with solid fiber results). The factor ϕ is the fraction of the nanotube occupied by wall material (*i.e.*, the volume fraction of nanotube walls with modulus $E_{zz}^{(f)}$ is $V_w = \phi V_f$).

The fiber efficiency factor, η_f, is a short fiber's load bearing capability relative to the analogous continuous fiber. It can be calculated from a concentric cylinders model (CCM) for a fiber of length l embedded in a matrix cylinder. The fiber has zero load on the ends while the matrix carries the entire applied load (see Fig. 1A). The efficiency factor is then defined by

$$\eta_f = \frac{1}{l\sigma_{zz}^{(f,\infty)}} \int_{-l/2}^{l/2} \left\langle \sigma_{zz}^{(f)}(z) \right\rangle dz \tag{2}$$

[☆]Accepted Author Manuscript (DOI:10.1016/j.compositesa.2011.08.012)

where $\left\langle \sigma_{zz}^{(f)}(z) \right\rangle$ is the average stress in the fibers and $\sigma_{zz}^{(f,\infty)}$ is the far-field fiber stress in the corresponding infinite concentric cylinders. The CCM problem is easily solved by shear lag analysis to give [1, 2, 3]:

$$\eta_f = 1 - \frac{\tanh \beta\rho}{\beta\rho} \tag{3}$$

where β is the dimensionless shear-lag parameter and $\rho = l/d$ is the fiber aspect ratio (for fiber diameter d). Since $\tanh x \to 1$ for large x, this equation has the limiting solution:

$$\rho(\eta_f) \approx \frac{1}{\beta(1-\eta_f)} \tag{4}$$

This limiting solution is accurate within 1% for $\eta_f \geq 0.7$. Thus, given any desired fiber efficiency and shear lag parameter, the fiber aspect ratio required to achieve that efficiency can easily be calculated. Here, 90% efficiency was arbitrarily selected as a benchmark for excellent short-fiber composites. The aspect ratio required to achieve this efficiency, denoted as ρ_{90}, is

$$\rho_{90} = \frac{10}{\beta} \tag{5}$$

This same criterion was used by Hull and Clyne [1]. It would be possible to account for additional stress transfer into the fibers ends, but for stiff fibers (relative to the matrix), the effect is always small.

The standard approach in the composites literature [1, 2] has made aspect ratio calculations by using the shear-lag parameter first derived by Cox [4]:

$$\beta_{\text{cox}} = 2\sqrt{\frac{G_m}{E_{zz}^{(f)} \ln \frac{1}{V_f}}} \qquad \text{which implies} \qquad \rho_{90}^{(\text{cox})} = 5\sqrt{2(1+\nu_m)\Big(-\ln V_f\Big)\frac{E_{zz}^{(f)}}{E_m}} \tag{6}$$

where $G_m = E_m/(2(1+\nu_m))$ is the shear modulus of the matrix and ν_m is its Poisson's ratio. This approach has two serious deficiencies. First, $\rho_{90}^{(\text{cox})}$ is independent of scale, which is a consequence of conventional elasticity analysis. A Cox-based analysis of nano-fiber reinforced polymers is pointless because it would provide nothing new compared to analysis of conventional fibers. Second, the Cox shear lag parameter can be shown by comparison to FEA calculations to be very inaccurate [3, 5]. Aspect ratio requirements predicted by β_{cox} are wrong by more than an order of magnitude. Shear lag analysis of fiber/matrix stress transfer can be much more accurate, such as the method first derived by Nayfeh [6] and later developed into modern stress-transfer theory by McCartney [7]. This improved shear lag solves the accuracy problem, but still has several deficiencies. First, the improved β is still scale invariant and thus provides no information unique to nanocomposites. Second, the analysis assumes a solid fiber and thus provides no information about hollow nanotubes. Third, the analysis breaks down at low fiber volume fracture and thus provides no guidance for work aimed at developing high-performance, low-fiber-volume-fraction nanocomposites.

This paper uses recent advances in fiber/matrix shear lag analysis [3, 5, 8] that extend the Nayfeh-McCartney approach to solve its deficiencies. The new shear-lag methods extend the analysis to handle multiple concentric cylinders and to handle a hollow core. This paper used these extensions to look at reinforcement effects of single-wall nanotubes (SWNT) and multi-wall nanotubes (MWNT) as compared to solid carbon fibers. More importantly, the new shear-lag methods can model imperfect interfaces (or interphases) between the matrix and the fiber or

between walls of a MWNT. The presence of an imperfect interphase introduces a scaling term that makes nanocomposites much different than conventional composites, and, for the first time, makes shear lag analysis a useful tool for modeling of nano-fiber composites. The interface term reveals effects that may be detrimental to nano-fiber reinforced composites. In other words, small-diameter fibers put more burden on the interface than large-diameter fibers. For effective nano-fiber reinforcement, the interface must be excellent. Finally, the new shear lag methods have solved the issue of low fiber volume fractions. This feature was used to evaluate the potential for low V_f nanocomposites with excellent properties. Such composites seem unlikely. Nanocomposite development would benefit more by emphasis on higher V_f composites.

2. Shear Lag Theory

First a remark. The fiber-efficiency-adjusted rule of mixtures in Eq. (1) is a common first step in short-fiber composite analysis [1, 2]. When η_f is found by a CCM analysis, the result is an upper bound to E_c^*. The CCM in Fig. 1A is a unit cell for a composite. When the CCM has the same V_f as the bulk composite, the full composite consists of repeating unit cells as illustrated in Fig. 1B. But, the composite can be built from CCM unit cells in many ways. An alternative is to imagine the CCM unit cell as having fiber volume fraction V_f^* that is higher than V_f in the bulk composite. The full composite then consists of CCM unit cells interspersed with pure matrix cells of length $l_m = (V_f^* - V_f)l/V_f$ such that the total composite fiber volume fraction remains V_f. The extreme geometry is when the CCM is pure fiber or $V_f^* = 1$ (see Fig. 1D). This last example has fiber and matrix elements in series that has the Reuss lower bound or series modulus. As V_f^* decreases from 1 to V_f the modulus transitions from this lower bound to the upper bound result. All calculations in this paper used the upper bound result, *i.e.*, used $V_f^* = V_f$. As a consequence, the η_f calculated here is the *upper bound* to fiber efficiency, which implies that ρ_{90} is a *lower bound* to the required aspect ratio. The benchmark term ρ_{90} thus defines the *minimum* fiber aspect ratio needed for a particular short fiber composite to be highly efficient. But, since axial properties are usually well modeled by upper bound results [9], this approach should provide a useful benchmark.

The CCM geometry for a SWNT in a matrix is shown in Fig. 1A. Here r_0 and r_f are the inner and outer radii of the SWNT wall and r_m is the outer radius of the matrix. The shear lag parameter, in dimensionless form and including imperfect interface effects is [3, 8]:

$$\beta^2 = \frac{B_{11} r_f^2}{A_{11}} \tag{7}$$

where

$$A_{11} = \frac{1}{2G_{zr}^{(f)}} \left\langle \left(1 - \frac{r_0^2}{r^2}\right) O_f(r) \right\rangle + \frac{1}{2G_m} \left\langle \left(\frac{r_m^2}{r^2} - 1\right) I_m(r) \right\rangle + \frac{1}{r_f D_s^{(f-m)}} \tag{8}$$

$$B_{11} = \frac{2}{E_{zz}^{(f)}(r_f^2 - r_0^2)} + \frac{2}{E_m(r_m^2 - r_f^2)} \tag{9}$$

where $G_{zr}^{(f)}$ and G_m are the fiber axial shear modulus (fiber is assumed orthotropic) and the matrix shear modulus (matrix is assumed isotropic), $O_f(r)$ and $I_m(r)$ are fiber and matrix shape functions, and $D_s^{(f-m)}$ is an imperfect interface parameter for the fiber-matrix interface.

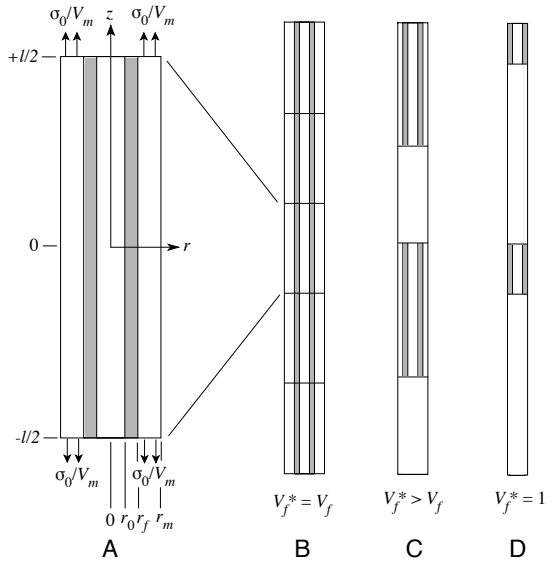

Figure 1: A. Cylindrical coordinate system for concentric cylinders model analysis for a single-wall nanotube of radius r_f (and core radius r_0) in a matrix cylinder of radius r_m under total applied stress σ_0, which is applied only to the matrix. The single wall is shaded gray; the core and matrix are both white. B. A composite structure made of a repeating unit cells of matrix and fiber. C. A composite structure made up of repeating unit cells having $V_f^* > V_f$ and regions of pure matrix such that the entire composite has fiber volume fraction V_f. D. Same as C except $V_f^* = 1$.

The imperfect interface model is based on Hashin's approach to modeling interfaces in composites [10, 11]. In brief, the modeled 2D fiber-matrix interface is allowed to have a displacement discontinuity. In shear lag analysis the only discontinuity that applies is relative sliding between the fiber and matrix. This axial displacement discontinuity, $[w]$, is then assumed to be proportional to the interfacial shear stress:

$$[w] = \frac{\tau_{rz}(r_f, z)}{D_s^{(f-m)}} \tag{10}$$

If $D_s^{(f-m)} \to \infty$, the discontinuity is zero and the interface is perfect. If $D_s^{(f-m)} \to 0$ the interfacial shear stress is zero and the interface is debonded. Values between 0 and ∞ define an imperfect interface with $D_s^{(f-m)}$ characterizing the interface quality. This interface modeling converts a 3D interphase zone into a 2D interface, which simplifies analysis and reduces the number of unknown interphase properties. In other words, a model with a 2D interface having interface property D_s gives approximate results for bulk composite response when compared to a model with an explicit 3D interphase. It achieves bulk response results with fewer interphase properties. If the real interphase zone has reduced stiffness (relative to fiber and matrix), the best 2D model would require a low D_s corresponding to slippage in the 2D view. If the real interphase was divided into pure fiber and matrix, the 2D model would be correct with $D_s = \infty$. It is also conceivable that interactions between a fiber and a matrix might stiffen the interphase region. The best approximation to a stiffened interphase zone in a model that has only a 2D interface might need a negative D_s. It is better viewed a $1/D_s^{(f-m)}$ that becomes zero for a perfect 2D interface, but may become negative for an interphase zone that is stiffened relative to other phases

[12] (note that negative D_s values are energetically admissible provided they correspond to an interphase zone with finite stiffness [12], *i.e.*, provided $1/D_s^{(f-m)}$ is greater than the result for a rigid interphase, which is negative).

Note that the role of interfacial properties on nanocomposite properties has often been the subject of papers on nanocomposites modeling (*e.g.*, [13, 14]), which usually have involved modifications of the Eshelby method for ellipsoidal inclusions [15] now with an interphase. The approach of this paper is to modify shear lag methods and account for interface effects using a single interfacial property, D_s. This new approach allows many shear-lag methods to be applied to nanocomposite modeling and reduces the role of the interface to a single property. As discussed below, it might be possible to measure D_s by experiments. In contrast, some modeling methods have been based on interfacial properties that are unknown and difficult to measure. Furthermore, a analysis involving cylindrical fibers may be the preferred approach to modeling fiber aspect ratio effects rather then analyses based on elliptical inclusions.

The functions $O_f(r)$ and $I_m(r)$ are shape functions for the fiber and matrix and the brackets $(< \cdots >)$ indicate an average over the fiber or matrix cross-sectional area. Any shape functions can be used with the only requirements being that $O_f(r_0) = 0$, $O_f(r_f) = I_m(r_f) = 1$, and $I_m(r_m) = 0$ [5]. McCartney suggested specific functions based on an assumed (and reasonable) radial dependence for the shear stress [7]:

$$O_f(r) = \frac{r^2 - r_0^2}{r_f^2 - r_0^2} \qquad \text{and} \qquad I_m(r) = \frac{r_m^2 - r^2}{r_m^2 - r_f^2} \tag{11}$$

After averaging, the shape function terms become:

$$\left\langle \left(1 - \frac{r_0^2}{r^2}\right) O_f(r) \right\rangle = \frac{r_0^2}{r_f^2 - r_0^2} \left(\frac{r_0^2}{r_f^2 - r_0^2} \ln \frac{r_f^2}{r_0^2} - 1 + \frac{r_f^2 - r_0^2}{2r_0^2} \right) \tag{12}$$

$$= \frac{1}{2} - \left(\frac{1-\phi}{\phi}\right)^2 \ln(1-\phi) - \left(\frac{1-\phi}{\phi}\right) \tag{13}$$

$$\left\langle \left(\frac{r_m^2}{r^2} - 1\right) I_m(r) \right\rangle = \frac{r_m^2}{r_m^2 - r_f^2} \left(\frac{r_m^2}{r_m^2 - r_f^2} \ln \frac{r_m^2}{r_f^2} - 1 - \frac{r_m^2 - r_f^2}{2r_m^2} \right) \tag{14}$$

$$= -\frac{1}{V_m} \left(\frac{V_m}{2} + 1 + \frac{1}{V_m} \ln(1 - V_m + \chi) \right) \tag{15}$$

where $\phi = (r_f^2 - r_0^2)/r_f^2$ and $V_m = (r_m^2 - r_f^2)/r_m^2$. The χ term in the $\ln(1 - V_m + \chi)$ term was included to make that term stable for V_m close to 1. Finite element analysis (FEA) calculations show that $\chi = 0.009$ is a universal constant that works for stress transfer into both isotropic and anisotropic fibers and for any fiber/matrix modulus ratio [5].

The full shear lag parameter becomes

$$\beta^2 = 4 \frac{\frac{1-V_m}{E_m V_m} + \frac{1}{E_{zz}^{(f)} \phi}}{\frac{1}{G_{zr}^{(f)}} \left(\frac{1}{2} - \left(\frac{1-\phi}{\phi}\right)^2 \ln(1-\phi) - \left(\frac{1-\phi}{\phi}\right) \right) - \frac{1}{G_m V_m} \left(\frac{V_m}{2} + 1 + \frac{1}{V_m} \ln(1 - V_m + \chi) \right) + \frac{2}{r_f D_s^{(f-m)}}} \tag{16}$$

Thus, the aspect ratio to get 90% efficiency from the fibers is

$$\rho_{90} = 5\sqrt{\frac{f_1(\phi)\frac{E_{zz}^{(f)}}{G_{zr}^{(f)}} + 2(1+\nu_m)f_2(V_f)\frac{E_{zz}^{(f)}}{E_m} + \frac{2E_{zz}^{(f)}}{r_f D_s^{(f-m)}}}{\frac{V_f}{1-V_f}\frac{E_{zz}^{(f)}}{E_m} + \frac{1}{\phi}}} \tag{17}$$

$$f_1(\phi) = \frac{1}{2} - \left(\frac{1-\phi}{\phi}\right)^2 \ln(1-\phi) - \left(\frac{1-\phi}{\phi}\right) \tag{18}$$

$$f_2(V_f) = -\left(\frac{1}{2} + \frac{1}{1-V_f} + \frac{1}{(1-V_f)^2}\ln\left(V_f + \chi\right)\right) \tag{19}$$

where ν_m is the Poisson's ratio of the matrix. ρ_{90} was written to use V_f and to emphasize key ratios, which are $E_{zz}^{(f)}/G_{zr}^{(f)}$, $E_{zz}^{(f)}/E_m$, and $E_{zz}^{(f)}/(r_f D_s^{(f-m)})$. The last ratio is the only one that contains a scaling factor or a fiber radius effect. The function $f_1(\phi)$ decreases smoothly from 0.5 to 0.0 as ϕ decreases from 1 (solid cylinders) to 0 (thin-walled cylinder). The function $f_2(V_f)$ decreases smoothly from 3.21 to 0.0 as V_f increases from 0 to 1. This function needs $\chi = 0.009$ for evaluation at $V_f = 0$, but χ should be changed to zero for $V_f > 0.5$. All calculations in this paper were for $V_f < 0.5$ and thus χ was kept at 0.009.

This author is biased that the shear-lag parameter from his work [3, 8], which is a extension of prior cylindrical shear lag models by Nayfeh [6] and McCartney [7] to include hollow fibers, to work at low V_f, and to model an imperfect interface, is the preferred shear lag model. This bias can be justified by the interface term, which introduces scaling effects and makes a shear-lag analysis worthwhile, and by its accuracy, which can be evaluated by comparison to finite element calculations (FEA). The average fiber stress from a shear lag analysis is [8]

$$\frac{\left\langle \sigma_{zz}^{(f)}(z)\right\rangle}{\sigma_{zz}^{(f,\infty)}} = 1 - \frac{\cosh\frac{\beta z}{r_f}}{\cosh\beta\rho} \tag{20}$$

This analytical solution is compared to FEA results for a hollow fiber in Fig. 2. The FEA comparison confirms that the shear lag analysis using β in Eq. (16) is extremely accurate for axial stresses and for both perfect and imperfect interfaces. The FEA analysis with an imperfect interface used the same Hashin [10, 11] interface model by using elements described in Ref. [12]. The normalizing far-field fiber stress was found by concentric cylinders analysis of infinite cylinders [9] (see the appendix).

Since the shear lag β in Eq. (16) is accurate, alternative shear lag parameters that differ are, by definition, inaccurate and should be avoided. One notable alternative parameter is found in the original (and often-cited) fiber/matrix shear lag analysis by Cox [4] (see Eq. (6)). Because β_{cox} is significantly smaller then β in Eq. (16), it predicts aspect ratio requirements that are an order of magnitude or more too high (depending on V_f). In brief, no new shear-lag application should be trusted until it is verified by FEA. The shear lag parameter used here was verified; the Cox parameter is inaccurate and therefore should never be used.

Some limiting results were found useful. First, most reinforcement is done by fibers that are much stiffer than the matrix. The stiff-fiber limit, defined as $E_{zz}^{(f)}\phi >> E_m$ and $G_{zr}^{(f)} >> E_m$, is

$$\rho_{90}^{(\text{stiff})} = \lim_{E_m << E_{zz}^{(f)}\phi,\ G_{zr}^{(f)}} \rho_{90} = 5\sqrt{\left(\frac{2E_m}{r_f D_s^{(f-m)}} + 2f_2(V_f)(1+\nu_m)\right)\frac{1-V_f}{V_f}} \tag{21}$$

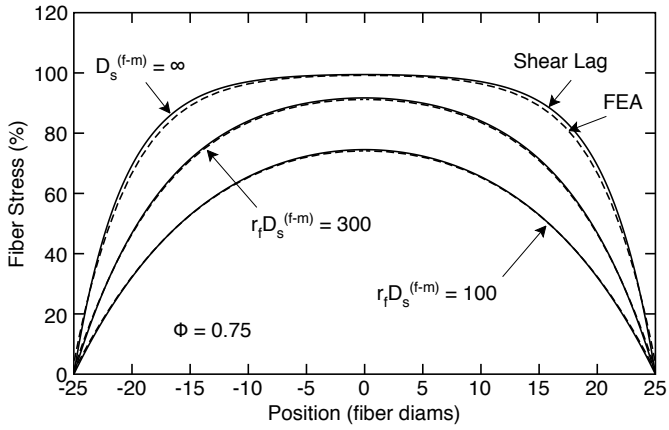

Figure 2: Average axial fiber stress (as percent of far-field fiber stress) as a function of position (in units of fiber diameters) by shear-lag analysis (solid curves) or by finite element analysis (dashed curves). The three curves are for three different values of $r_f D_s^{(f-m)}$ in units of MPa. These calculations used $E_m = 2500$ MPa, $\nu_m = 0.33$, $E_{zz}^{(f)}/E_m = 400$, $E_{zz}^{(f)}/G_{zr}^{(f)} = 10$, $r_f = 1$ μm, $r_0 = 0.5$ μm, $\phi = 0.75$, $\rho = 50$, and $V_f = 0.02$.

This stiff limit depends only on matrix properties, the interface quality, and the fiber radius. It is independent of other fiber properties including whether the fiber is solid or hollow (*i.e.*, independent of ϕ). This stiff-fiber limit is infinite as $V_f \to 0$, but the full Eq. (17) is well-behaved as $V_f \to 0$ for any fiber stiffness. The result is:

$$\rho_{90}^{(0)} = \lim_{V_f \to 0} \rho_{90} = 5\sqrt{\phi\left(f_1(\phi)\frac{E_{zz}^{(f)}}{G_{zr}^{(f)}} + 6.42(1+\nu_m)\frac{E_{zz}^{(f)}}{E_m} + \frac{2E_{zz}^{(f)}}{r_f D_s^{(f-m)}}\right)} \tag{22}$$

3. Results

3.1. Single Wall Nanotubes with Perfect Interface

This section considers SWNTs compared to solid AS4 carbon fibers when the interface is perfect ($D_s^{(f-m)} = \infty$). When the interface is perfect, the shear-lag parameter is scale invariant meaning the only differences between SWNTs and large, solid fibers are their moduli and the ϕ factor. The key SWNT properties are its radius and wall thickness and its tensile and shear moduli. Wall thickness estimates vary from 0.066 nm to 0.69 nm [16]; here the thickness was assumed to be the interlayer graphite spacing or 0.34 nm [16]. The SWNT radius was set to $r_f = 0.75$ nm or an average of SWNTs with diameters between 1 and 2 nm. These assumptions resulted in $r_0 = 0.41$ and $\phi = 0.701$. Reports on the axial modulus of SWNTs vary from 220 GPa to 4150 GPa [17]. All calculations here were for reinforcing a typical glassy polymer with $E_m = 2.5$ GPa and $\nu_m = 0.33$; thus $E_{zz}^{(f)}/E_m$ is between 88 and 1660. The $E_{zz}^{(f)}/G_{zr}^{(f)}$ ratio requires knowledge of the SWNT axial shear modulus, which is unknown (note: for orthotropic materials $G_{zr}^{(f)}$ is different than a shear modulus that could be determined by torsion experiments (*i.e.*, $G_{z\theta}^{(f)}$), but it might be similar). Here, $E_{zz}^{(f)}/G_{zr}^{(f)}$ was assumed to be the same as it is for solid AS4 carbon fibers or $E_{zz}^{(f)}/G_{zr}^{(f)} = 220/14 = 15.7$. This assumption had virtually no influence on the calculations and thus the $E_{zz}^{(f)}/G_{zr}^{(f)}$ value is relatively unimportant. This observation might

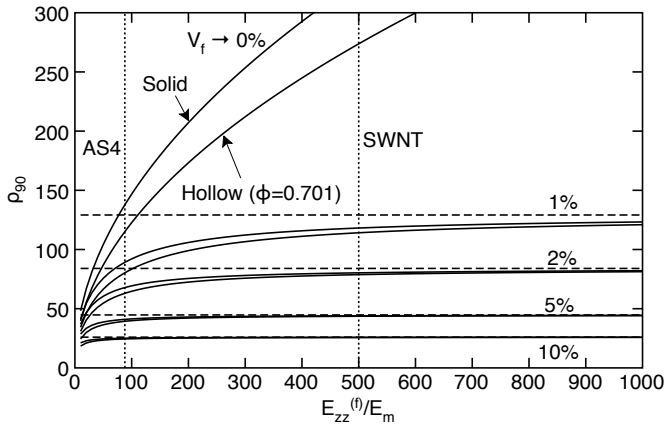

Figure 3: The minimum fiber aspect ratio, ρ_{90}, as a function of $E_{zz}^{(f)}/E_m$ for various fiber volume fractions. The two solid curves at each volume fraction are for solid fibers ($\phi = 1$) or hollow fibers ($\phi = 0.701$) (using Eq. (17)). The dashed lines for $V_f \geq 1\%$ are the stiff fiber limit, $\rho_{90}^{(\text{stiff})}$ (using Eq. (21)). The vertical dotted lines are expected $E_{zz}^{(f)}/E_m$ ratios for AS4 or SWNT fibers.

change if SWNTs were found to have an anomalously low $G_{zr}^{(f)}$. The solid AS4 carbon fiber properties are $r_f = 3500$ nm, $E_{zz}^{(f)} = 220$ GPa, $E_{zz}^{(f)}/G_{zr}^{(f)} = 15.7$, and $\phi = 1$.

Figure 3 plots the minimum fiber aspect ratio (ρ_{90}) as a function of $E_{zz}^{(f)}/E_m$ for solid and hollow (with the assumed $\phi = 0.701$) fibers for several volume fractions. The minimum aspect ratio increases as $E_{zz}^{(f)}/E_m$ increases, but at a decreasing rate as V_f increases. Comparing volume fractions, the fiber aspect ratio requirements are high for low V_f, but decrease dramatically for higher V_f. The horizontal dashed lines are the stiff fiber limits. Each volume fraction asymptotically approaches the stiff limit. For $V_f \geq 5\%$, the stiff fiber limit gives a reasonable approximation for reinforcement by any stiff fiber. No stiff limit is plotted for $V_f \to 0\%$ because $\lim_{V_f \to 0} \rho_{90}^{(\text{stiff})} = \infty$. The figure instead plots $\rho_{90}^{(0)}$; this low V_f limit shows the highest required fiber aspect ratio, which continues to increase as $E_{zz}^{(f)}/E_m$ increases.

Each volume fraction in Fig. 3 has one curve for solid fiber and another for hollow fiber. The solid curve is always slightly higher. The vertical dashed lines show possible $E_{zz}^{(f)}/E_m$ for AS4 or SWNT fibers (with $E_{zz}^{(f)} = 1250$ GPa), respectively. Although the solid ρ_{90} curves are always *higher* than the hollow curves, the intersection of the AS4 properties with the solid curve is always *lower* than the intersection of the SWNT properties with the hollow curve. This difference, however, depends on V_f — the fiber aspect ratio intersections for SWNTs are essentially identical to those for AS4 fiber intersections for $V_f \geq 5\%$, but are slightly higher for $V_f < 5\%$. The largest difference, which may reach a factor of 2, occurs in the limit as $V_f \to 0\%$. In other words, ρ_{90} is rather weakly dependent on ϕ except at low V_f. ρ_{90} for SWNTs would decrease further if ϕ was less than 0.701 as assumed here, but within the range of possible SWNT shapes, the effect is expected to be small. The much larger effect of ϕ is as a scaling term in Eq. (1), where contribution of SWNT modulus to composite modulus is directly reduced by any reduction in ϕ.

The volume fraction effects for AS4 and SWNT fibers are plotted in Fig. 4. The three curves for $D_s^{(f-m)} = \infty$ are the perfect interface results. The AS4 and SWNT fiber aspect ratio requirements are virtually identical for $V_f \geq 5\%$. For $V_f < 5\%$, SWNT composites would require slightly higher aspect ratio for excellent reinforcement. At high volume fractions ($V_f > 20\%$)

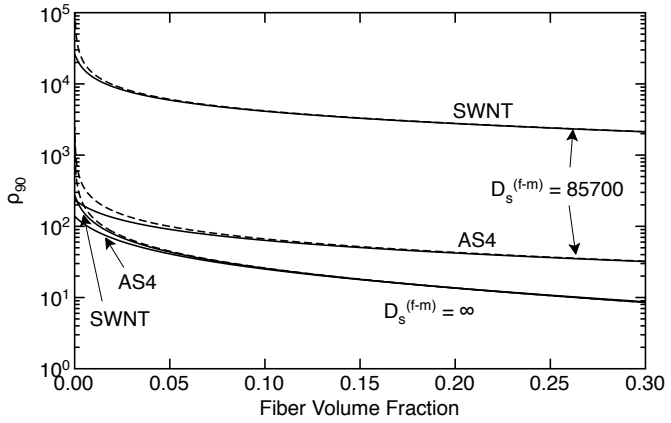

Figure 4: The minimum fiber aspect ratio, ρ_{90}, as a function of V_f for AS4 and SWNT fibers. The $D_s^{(f-m)} = \infty$ curves are for a perfect interface. The $D_s^{(f-m)} = 85700$ (units of MPa/mm) curves are for an imperfect interface. The dashed lines are the stiff fiber limit, $\rho_{90}^{(\text{stiff})}$.

the fiber aspect ratios become rather modest — $\rho_{90} < 10$; thus short fibers should reinforce more effectively at higher V_f. The dashed line is the stiff fiber limit. It is an excellent approximation for SWNT for $V_f \geq 2\%$ and for AS4 for $V_f \geq 5\%$.

3.2. Single Wall Nanotubes with Imperfect Interface

The evaluation of imperfect interface effects requires knowledge of the interface parameter $D_s^{(f-m)}$. The most direct way to measure $D_s^{(f-m)}$ is to measure stress transfer into a single fiber. The results will resemble the axial stresses in Fig. 2. If the fiber and matrix properties are known, stress analysis can be used to determine $D_s^{(f-m)}$. This technique was used on HM carbon fibers embedded in an epoxy matrix. The fiber axial strains were measured by Raman spectroscopy [18] and interpreted using a Bessel-Fourier analysis [19] resulting in a measured $r_f D_s^{(f-m)} = 300$ MPa [18] (note that D_s in Refs. [18] and [19] is equivalent to $r_f D_s^{(f-m)}$ used here and defined by Hashin [10]). These same experimental results were reanalyzed by the shear-lag analysis used here, which gave the same $r_f D_s^{(f-m)} = 300$ MPa [5]. Using $r_f = 3.5$ μm results in $D_s^{(f-m)} = 85700$ MPa/mm. Imperfect interface theory implies that $D_s^{(f-m)}$ is an interface property that is independent of the fiber radius. There are no experimental results as a function of fiber radius, however, to know for sure. The following calculations assumed $D_s^{(f-m)}$ is a material property and that it is the same for AS4 fibers and SWNTs as it is for HM fibers.

Figure 4 plots the AS4 and SWNT fiber aspect ratio requirements with $D_s^{(f-m)} = 85700$ MPa/mm. An imperfect interface means that higher aspect ratios are needed before effective reinforcement can be realized. For AS4 fibers, ρ_{90} increased 2–4 fold, depending on V_f. In contrast, for SWNTs, ρ_{90} increased 100–250 fold, depending on V_f. The dramatic effect for SWNTs is caused by their small r_f, and the presence of r_f in the denominator of the imperfect interface term. In brief, the interface effects with small-diameter fibers, such as SWNTs, are much more prominent than in larger-diameter fibers. If the SWNT interface is similar to the HM fiber interface, then SWNTs are unlikely to ever produce effectively reinforced short fiber composites.

It is possible, however, that $D_s^{(f-m)}$ for SWNTs may be dramatically different. First, $D_s^{(f-m)}$ may not be a material property. The experiments needed to answer this question are to measure $D_s^{(f-m)}$ as a function of fiber radius for a series of otherwise identical fibers. Second, SWNTs may have much more favorable interactions with some matrices than HM fibers have with epoxy. For example a SWNT might constrain an interphase region inducing a stiffening effect that could result in a negative $D_s^{(f-m)}$. If such an effect occurs, ρ_{90} would be similar to the perfect interface results, or perhaps slightly lower. Conversely, a negative interaction between a SWNT and a matrix that results in a compliant interphase would be an extremely poor choice for a nano-fiber composite. Note that negative $D_s^{(f-m)}$ values are limited to the condition that β remain real. Thus the physically accessible range for $D_s^{(f-m)}$ is

$$\frac{1}{D_s^{(f-m)}} > -\frac{r_f}{2}\left(\frac{f_1(\phi)}{G_{zr}^{(f)}} + \frac{f_2(V_f)}{G_m}\right) \tag{23}$$

The lower limit corresponds to instant stress transfer (*i.e.*, a rigid interphase) with $\beta = \infty$ and $\rho_{90} = 0$.

3.3. Multiwall Nanotubes

A MWNT shear lag analysis could be constructed using a model of multiple concentric cylinders and it could account for slippage (or telescoping) between the cylinders by adding an interface parameter for wall-to-wall contact — $D_s^{(w-w)}$ [3, 5]. Assuming the various walls have the same mechanical properties as a SWNT wall, the only new parameter would be $D_s^{(w-w)}$. This complicated, multicylinder analysis, however, is unnecessary. The MWNT results would clearly fall between the SWNT results for outer wall only (if $D_s^{(w-w)} \to 0$) and SWNT results that considered all walls as one solid wall (if $D_s^{(w-w)} \to \infty$). Since the results in Figs. 3 and 4 show little effect on the diameter of the core, the MWNT fiber aspect ratio requirements must be virtually identical to those of SWNTs.

Once the fiber aspect ratio requirements are met, the overall composite modulus depends on the product $E_{zz}^{(f)}\phi$. For SWNT, ϕ is calculated from radius and wall thickness. For MWNTs, the effective ϕ depends on $D_s^{(w-w)}$. If the walls are free to slip, or telescope under strain, that would imply that $D_s^{(w-w)} \approx 0$. In this limit, the inner walls would carry no stress and the effective ϕ should be determined from r_f and the inner radius of the *outer-most* wall. On the other hand, if the walls are perfectly bonded, the effective ϕ should be calculated from r_f and the inner radius of the *inner-most* wall. For partial bonding the effective ϕ would be between these two limits. Most descriptions of MWNT suggest that slippage is more likely than perfect bonding. Thus composites of MWNTs are more likely to reinforce as if they were SWNTs made by removing the inner walls.

4. Discussion and Conclusions

A simple shear lag analysis of concentric cylinders, when done accurately, provides useful results about fiber aspect ratio requirements in short fiber composites and about the effective modulus of aligned short fiber composites. A particularly simple result for aspect ratio is the stiff limit or $\rho_{90}^{(\text{stiff})}$ (see Eq. (21)). This stiff limit is very accurate for $V_f > 5\%$. Even for $V_f < 5\%$ it is sufficiently accurate that it gives useful results; it is probably not worth the effort to determine the extra material properties required to use the full ρ_{90} (see Eq. (17)). It cannot be used in the limit $V_f \to 0$, but then $\rho_{90}^{(0)}$ (see Eq. (22)) can be used instead. Based on $\rho_{90}^{(\text{stiff})}$, the fiber aspect ratio

requirement depends on fiber volume fraction. It is highest for low V_f and decreases significantly at higher V_f. The only fiber and matrix properties that affect $\rho_{90}^{(\text{stiff})}$ are the group $E_m/(r_f D_s^{(f-m)})$. This term is an interphase effect. The presence of r_f in the denominator is a scaling effect that could be detrimental to nanocomposites. In other words, the interface quality is more important in nanocomposites than in composites with micron or larger sized fibers. One should not expect excellent SWNT composites unless $1/D_s^{(f-m)}$ is close to zero or slightly negative.

Once aspect ratio requirements are met, the criterion used here implies that $\eta_f \geq 0.9$. The final composite modulus then depends on E_m, V_f and the product $E_{zz}^{(f)}\phi$ (see E_c^* in Eq. (1)), which is a reduced modulus that is more important to composite properties than is the wall modulus, $E_{zz}^{(f)}$. The reduced modulus can be determined from force-displacement experiments on SWNTs by normalizing to the entire cross-sectional area rather then the area of the wall material (*i.e.*, an easier experiment then determining $E_{zz}^{(f)}$ because it does not require determination of the wall thickness). For practical applications, $E_{zz}^{(f)}\phi$ should be reported along with $E_{zz}^{(f)}$ results. For MWNTs, $E_{zz}^{(f)}\phi$ should use an *effective* ϕ that accounts for contribution of the interior walls. This effective ϕ will be between the result based on the outer wall alone and the result that includes all walls.

The E_c^* in Eq. (1) is for aligned, short-fiber composites, which are uncommon materials. But, given results for aligned short-fiber composites, 2D or 3D random composite properties can be evaluated by suitable 2D [20] and 3D [21] averaging methods. The resulting random composite moduli scale with E_c^* and thus calculations here are relevant to both aligned and random composites. Because E_c^* is an upper bound modulus, the averaging method also gives an upper bound for the random composite. By definition, an upper bound modulus is the highest possible modulus for all possible structures. In other words, all structures, including percolated geometries, must have a lower modulus. The idea that percolation can provide unexpected properties that violates upper bounds is a misconception.

One claimed SWNT potential is that because of their remarkable moduli, they could produce stiff composites at very low fiber volume fraction. Fiber aspect ratio requirements, however, suggest this potential is unlikely to be realized. As V_f decreases, the required aspect ratio increases. In the limit $V_f \to 0$, it increases further as $E_{zz}^{(f)}$ increases. In other words, reinforcement is always less effective at low V_f. Better potential for nanocomposites is more likely at higher V_f, where the aspect requirements are much smaller — ρ_{90} can be below 10 for V_f around 25%. The interface is still critical, but favorable SWNT/matrix interactions might stiffen the interphase and lead to better composites than could be obtained with larger-diameter fibers. These low aspect ratio requirements at higher V_f are lower than prior calculations for short fiber composites (*e.g.*, $\rho_{90} \sim 100$ [1], which is too high because it used β_{cox}). Recall, however, that this new ρ_{90} is a lower bound. Real materials might require a higher aspect ratio, but the aspect ratio needed should decrease as V_f increases.

The importance of the interface and the lack of experimental results for $D_s^{(f-m)}$ suggests it would be beneficial to develop a method to measure interface quality. The best experiment is to directly measure stress transfer into a single fiber using Raman methods [18]. That approach, however, only works for certain fibers and is beyond the resolution of Raman for SWNTs. One possible alternative would be to make a series of aligned short-fiber composites with varying fiber aspect ratio. Two options for characterizing the composites would be to measure the modulus or to use Raman to measure an average fiber strain. Either of these results would provide an experimental estimate of η_f. With known fiber and matrix properties, the only unknown in η_f would be the interfacial parameter.

Finally, this paper's analysis assumes that continuum mechanics for stress transfer applies to SWNTs. In other words, assuming continuum mechanics is appropriate, what can be said about the fiber aspect ratio requirements and composite modulus of SWNT reinforced polymers? Such modeling can guide nanocomposite development. Two key findings here are that fiber aspect ratio requirements are modest, but only at higher V_f, and that the interface is important. Experiments should focus on higher V_f composites and developing new interface characterization methods. The alternative is to assume that some undiscovered "nano" effect exists and therefore low V_f composites with remarkable properties are possible. The nature of "undiscovered" phenomena, however, is that they might not exist or if they do exist, they might be detrimental rather then beneficial.

Appendix

The far-field fiber stress was found by a concentric cylinder analysis for infinite length cylinders [9] amended to allow for a hollow fiber. The FEA calculations here were done for a transversely isotropic fiber. The results for such fibers are

$$\sigma_{zz}^{(f,\infty)} = \left(E_A + \frac{4\nu_A V_m(\nu_A - \nu_m)}{\frac{V_m}{k_T} + \frac{V_f\phi}{k_m} + \frac{\phi}{G_m} - \frac{\phi}{G_T}} \right) \frac{\sigma_{app}}{E_A^*} \tag{24}$$

where E_A^* is the effective axial modulus of the concentric cylinders:

$$E_A^* = E_A V_f \phi + E_m V_m + \frac{4V_m V_f \phi(\nu_A - \nu_m)^2}{\frac{V_m}{k_T} + \frac{V_f\phi}{k_m} + \frac{\phi}{G_m} - \frac{\phi}{G_T}} \tag{25}$$

Here σ_{app} is the total applied stress, E_A, ν_A, k_T, and G_T are axial modulus, axial Poisson's ratio, transverse bulk modulus, and shear modulus of the transversely isotropic fiber and E_m, ν_m, k_m, and G_m are the same properties for the isotropic matrix. V_f, V_m, and ϕ are as defined in the text of this paper. In these equations, the first terms dominate while the second terms account for small effects due to Poisson's ratio difference between the fiber and the matrix. A similar analysis could be done for orthotropic fibers, but results in considerably more complicated expressions. The solid fiber results in Ref. [9] are recovered by setting $\phi = 1$ and eliminating the G_T term.

References

[1] D. Hull, T. W. Clyne, An Introduction to Composite Materials, 2nd Edition, Cambridge University Press, 1996.

[2] M. R. Piggott, Load Bearing Fibre Composites, 2nd Edition, Kluwer Academic Publishers, 2002.

[3] J. A. Nairn, On the use of shear-lag methods for analysis of stress transfer in unidirectional composites, Mech. of Materials 26 (1997) 63–80.

[4] H. L. Cox, The elasticity and strength of paper and other fibrous materials, Brit. J. Appl. Phys. 3 (1952) 72–79.

[5] J. A. Nairn, Generalized shear-lag analysis including imperfect interfaces, Advanced Composite Letters 13 (2004) 263–274.

[6] A. H. Nayfeh, Thermomechanically induced interfacial stresses in fibrous composites, Fibre Sci. & Tech. 10 (1977) 195–209.

[7] L. N. McCartney, Analytical models of stress transfer in unidirectional composites and cross-ply laminates, and their application to the prediction of matrix/transverse cracking, in: J. N. Reddy, K. L. Reifsnider (Eds.), Local Mechanics Concepts for Composite Material Systems, 1992, pp. 251–282.

[8] J. A. Nairn, D.-A. Mendels, On the use of planar shear-lag methods for stress-transfer analysis of multilayered composites, Mechanics of Materials 33 (2001) 335–362.

[9] Z. Hashin, Analysis of properties of fiber composites with anisotropic constituents, J. Appl. Mech. 46 (1979) 543–549.
[10] Z. Hashin, Thermoelastic properties of fiber composites with imperfect interface, Mech. of Materials 8 (1990) 333–348.
[11] Z. Hashin, Extremum principles for elastic heterogenous media with imperfect interfaces and their application to bounding of effective moduli, Journal of the Mechanics and Physics of Solids 40 (4) (1992) 767–781.
[12] J. A. Nairn, Numerical implementation of imperfect interfaces, Computational Materials Science 40 (2007) 525–536.
[13] H. L. Duan, J. Wang, Z. P. Huang, B. L. Karihaloo, Eshelby formalism for nano-inhomogeneities, Proc. Roy. Soc. Lond. A 461 (3335–3353).
[14] P. Sharma, S. Ganti, Size-dependent eshelby's tensor for embedded nano-inclusions incorporating surface/interface energies, Journal of Applied Mechanics 71 (5) (2004) 663–671. doi:10.1115/1.1781177.
URL http://link.aip.org/link/?AMJ/71/663/1
[15] J. D. Eshelby, The determination of the elastic field of an ellipsoidal inclusion and related problems, Proc. R. Soc. Lond. A 241 (1957) 376–396.
[16] Y. Huang, J. Wu, K. C. Hwang, Thickness of graphene and single-wall carbon nanotubes, Phys. Rev. B 74 (24) (2006) 245413. doi:10.1103/PhysRevB.74.245413.
[17] Y. Huang, R. J. Young, Interfacial micromechanics in thermoplastic and thermosetting matrix carbon fibre composites, Composites Part A 27A (1996) 973–980.
[18] A. Paipetis, Y. C. Liu, C. Galiotis, J. A. Nairn, Stress transfer from the matrix to the fiber in a fragmentation test: Raman experiments and analytical modeling, J. Comp. Mat. 33 (1999) 377–399.
[19] J. A. Nairn, Y. C. Liu, C. Galiotis, Analysis of stress transfer from the matrix to the fiber through an imperfect interface: Application to raman data and the single-fiber fragmentation test, in: C. J. Spragg, L. T. Drzal (Eds.), ASTM STP 1290, 1995, pp. 47–65.
[20] J. Halpin, J. Kardos, Moduli of crystalline polymers employing composite theory, Journal of Applied Physics 43 (5) (1972) 2235–2241. doi:10.1063/1.1661482.
[21] R. M. Christensen, Mechanics of Composite Materials, John Wiley & Sons, New York, 1979.